Challenge Journal of
STRUCTURAL MECHANICS

Research Article

Finite element investigation of the cyclic behavior of bolted extended end plate connections strengthened with longitudinal plates

Orkun Yılmaz [a,*], Zeynep Ünsal Aslan [b]

[a] *Department of Civil Engineering, Yildiz Technical University, 34220 İstanbul, Türkiye*
[b] *Department of Civil Engineering, Batman University, 72100 Batman, Türkiye*

ABSTRACT

The cyclic behavior of bolted extended end plate beam-to-column connections strengthened with longitudinal plates parallel to the beam web was investigated through three-dimensional nonlinear finite element analysis. Unlike previously studied methods such as haunches, end plate stiffeners, side plates, and internal reinforcement details, this strengthening configuration places the plates within the beam depth and parallel to the beam web, an arrangement that has not been systematically examined for this connection type. The finite element model was first validated using results from a benchmark experimental test reported in the literature. Following validation, six connection configurations were analyzed under the AISC cyclic loading protocol. These included a four-bolt unstiffened end plate (4E) reference model, a four-bolt stiffened end plate (4ES) model, and four models incorporating longitudinal plates with varying plate lengths and locations. The numerical results were assessed based on hysteretic response, cumulative energy dissipation, bolt force distribution, equivalent plastic strain development, and equivalent viscous damping. It was observed that the addition of longitudinal plates improved the global cyclic response by increasing the moment capacity while maintaining stable hysteresis loops. However, increasing the length of the longitudinal plates resulted in higher tensile force demands on the bolts, indicating the need for careful design to avoid brittle failure modes. Analysis of the equivalent plastic strain showed that the longitudinal plates reduced the peak strain in the beam-end region by up to approximately 64% relative to the unstiffened (4E) reference connection, whereas the conventional stiffener (4ES) shifted the plastic hinge away from the column face but produced the highest strain concentration. The results indicate that the longitudinal plate detail offers a practical strengthening approach for improving the cyclic response of bolted extended end plate connections, provided that the increased bolt tensile demand is explicitly considered in design.

ARTICLE INFO

Article history:
Received – April 12, 2026
Revision requested – May 26, 2026
Revision received – July 7, 2026
Accepted – July 14, 2026

Keywords:
Bolted extended end plate connection
Cyclic behavior
Finite element analysis
Longitudinal plate strengthening
Seismic performance
Beam-to-column connection

Citation: Yılmaz O, Ünsal Aslan Z (2026). Finite element investigation of the cyclic behavior of bolted extended end plate connections strengthened with longitudinal plates. *Challenge Journal of Structural Mechanics*, 12(3), 225–241.

1. Introduction

Steel moment-resisting frames are commonly utilized in seismic regions due to their inherent ductility and capacity for energy dissipation through stable inelastic mechanisms. In these systems, bolted end plate beam-to-column connections are frequently selected because they simplify fabrication, minimize field welding, and are suitable for both new construction and retrofit scenarios. The behavior of end plate joints is determined by a combination of factors, including end plate bending, column-flange flexibility, bolt pretension, prying action, lo-

* *Corresponding author.* E-mail address: yilmazo@yildiz.edu.tr (O. Yılmaz)
ISSN: 2149-8024 / DOI: https://doi.org/10.20528/cjsmec.2026.1162

cal contact conditions, and force redistribution within the joint region. These factors collectively influence the stiffness, strength, rotational capacity, and failure mode of the connection, as established in previous studies (Bahaari and Sherbourne 1996; Bursi and Jaspart 1998; Troup et al. 1998; Abidelah et al. 2012; Prinz et al. 2014).

A significant body of research has addressed haunch-based strengthening methods. Experimental results by Lee et al. (2003) demonstrated that welded straight haunches are effective in relocating plastic hinging away from the column face and enhancing cyclic performance, provided that detailing is appropriate. Saberi et al. (2019) further showed that welded haunches can rehabilitate weak bolted end plate connections, with their effectiveness being highly dependent on haunch thickness and angle. Zhao et al. (2021) reported that haunch retrofitting increases both moment resistance and initial rotational stiffness, while also modifying the internal force-transfer mechanism within the joint. Collectively, these studies confirm the effectiveness of haunches, but also highlight that their performance is highly sensitive to geometric parameters and may not always achieve an optimal balance between ductility, force redistribution, and constructability.

Stiffeners, side plates, and cover-plate-type reinforcement represent another principal research focus. Herath et al. (2023) emphasized that the performance of bolted stiffened end plate connections is governed not only by resistance but also by the hierarchy of yielding and the specific performance objectives. El-Sa'eed (2024) investigated side-plate strengthening and observed significant increases in moment capacity, though these solutions require additional fabrication and welding. For portal-frame applications, Zhang et al. (2024, 2025a, 2025b) introduced prefabricated retrofit systems utilizing cover plates and channel-type components, demonstrating improvements in strength and initial stiffness, as well as reductions in end plate opening and bolt demand under certain conditions. However, these studies also noted that excessive reinforcement can transfer damage to other components, increase bolt force demand, or compromise the balance between strength enhancement and cyclic performance. Similarly, Yılmaz and Bekiroğlu (2016) showed numerically that reinforcing the panel zone of bolted end plate connections reduces plastic strains in the panel zone but can result in earlier beam flange or web buckling and decreased rotational capacity.

Another group of studies has focused on internal strengthening details for end plate joints connected to hollow or closed-section columns. Zhang et al. (2021) demonstrated that measures such as infilled concrete and facing plates can enhance the stiffness and moment capacity of one-sided bolted end plate connections to hollow square columns. Cai et al. (2022) showed that end plate stiffeners and internal strengthening components improve seismic performance by facilitating force transmission and increasing rotational capacity. Liu et al. (2022) reported that novel internal strengthening structures have a significant impact on failure sequence, bolt-force development, and cyclic energy dissipation. It should be noted that these studies primarily address hollow-section connection configurations, rather than conventional open-section bolted extended end plate beam-to-column joints. In a related study, Yılmaz and Bekiroğlu (2022) examined the biaxial cyclic behavior of a bolted end plate connection to an I-column modified with box-plates parallel to the column web, and found that the proposed detail exhibited acceptable hysteretic behavior under cyclic loading. However, this investigation focused on a reformed weak-axis connection detail under biaxial loading, rather than on strengthening conventional extended end plate joints using beam-side longitudinal plates.

In addition to strengthening studies, extensive research has addressed the mechanics of end plate connections and their individual components. The behavior of T-stub components, prying action, bolt pretension, and three-dimensional force transfer has been thoroughly investigated through analytical, experimental, and finite element approaches (Yang and Lee 2007; Hu et al. 2011; Peng et al. 2018; Ghamari et al. 2023; Couchaux and Madhouni 2022; Taheripour et al. 2022; Zhang et al. 2023; Xiao et al. 2024; Liu et al. 2025). These studies collectively indicate that strengthening strategies must be evaluated not only for their effect on resistance, but also for their impact on force redistribution, local deformation demand, prying action, and cyclic stability.

Although a wide range of strengthening approaches has been reported, most studies have focused on haunches, end plate stiffeners, side plates, cover-plate assemblies, and internal reinforcement details. In contrast, the application of longitudinal plates welded within the beam depth, between the beam flanges, and oriented parallel to the beam web has not been systematically examined for bolted extended end plate connections. This configuration differs from conventional end plate stiffeners in that it does not introduce an upward projection above the beam top flange, which can be advantageous for architectural and detailing considerations. Furthermore, because the longitudinal plates are aligned with the beam web rather than concentrated in the extended end plate region, this arrangement may provide a more distributed strengthening effect and a more favorable balance among moment resistance, bolt-force development, cyclic stability, and ductile deformation.

In the present study, a novel strengthening concept is introduced, in which longitudinal plates are installed between the beam flanges and parallel to the beam web. The main objective is to determine whether this strengthening configuration can enhance the hysteretic response and the energy dissipation capacity of bolted extended end plate connections, while also evaluating its influence on bolt-force demand and force redistribution within the connection region. For this purpose, detailed three-dimensional nonlinear finite element models were developed and subjected to cyclic loading, and the influence of plate geometry and placement on the seismic performance of the connection was systematically evaluated.

2. Finite Element Models

2.1. Connection configurations

Six finite element models of beam-to-column connections were established and analyzed using Ansys Finite Element Analysis Software (ANSYS 2024) to evaluate the influence of longitudinal plates on the cyclic performance of bolted extended end plate connections. The general geometry and main dimensions of the models are shown in Fig. 1, and the detailed configurations of the connection models are provided in Fig. 2. Table 1 summarizes the nomenclature of all models.

Each model consisted of an IPE270 beam connected to an HE240B column. Both sections meet the requirements for seismically compact members as specified in ANSI/AISC 341-16 (AISC 2016). The first model is a four-bolt unstiffened extended end plate connection (4E), and the second model is a four-bolt stiffened extended end plate connection (4ES). Both connections were designed in accordance with ANSI/AISC 358-22 (AISC 2022a). The required end plate thicknesses were determined as 25 mm for the 4E connection and 22 mm for the 4ES connection. M20 bolts were used in both configurations.

The remaining four models were developed by modifying the 4E connection through the addition of longitudinal plates positioned between the beam flanges and parallel to the beam web. These models were established to investigate the effects of plate length and plate location on the connection behavior. In the adopted nomenclature, 'N' indicates that the longitudinal plates are welded near the beam web, while 'O' indicates that the plates are welded to the flange tips.

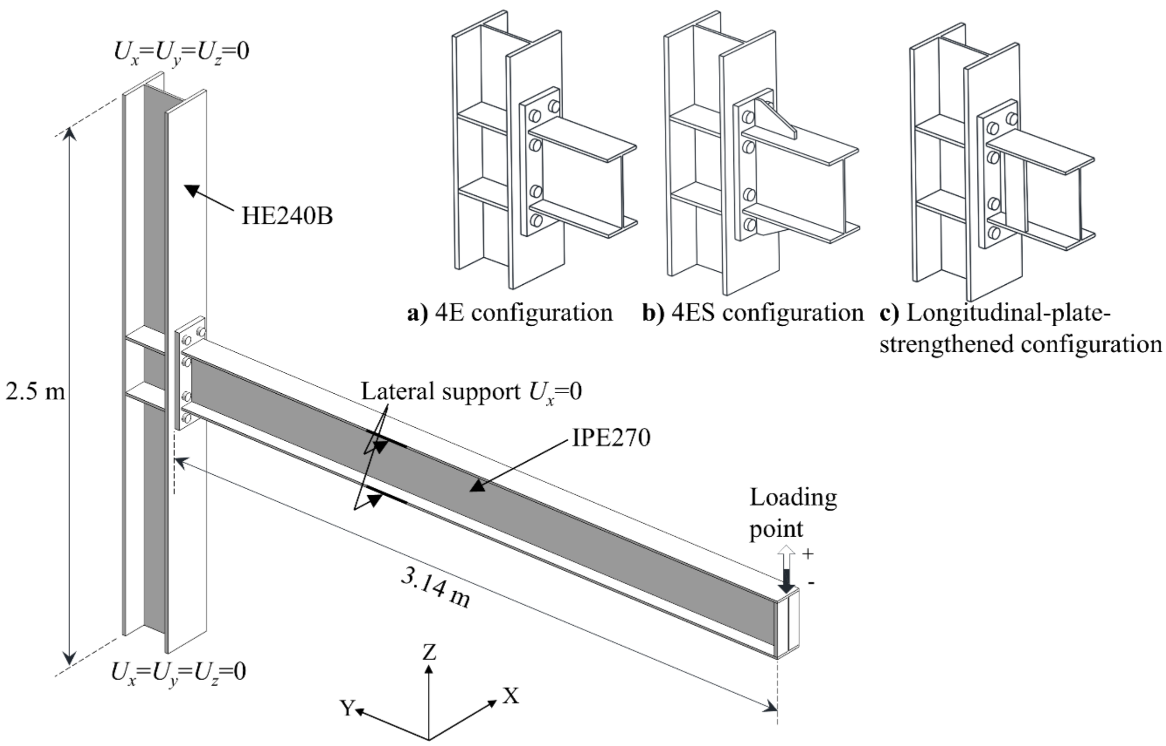

Fig. 1. The overall geometry and principal dimensions of the models.

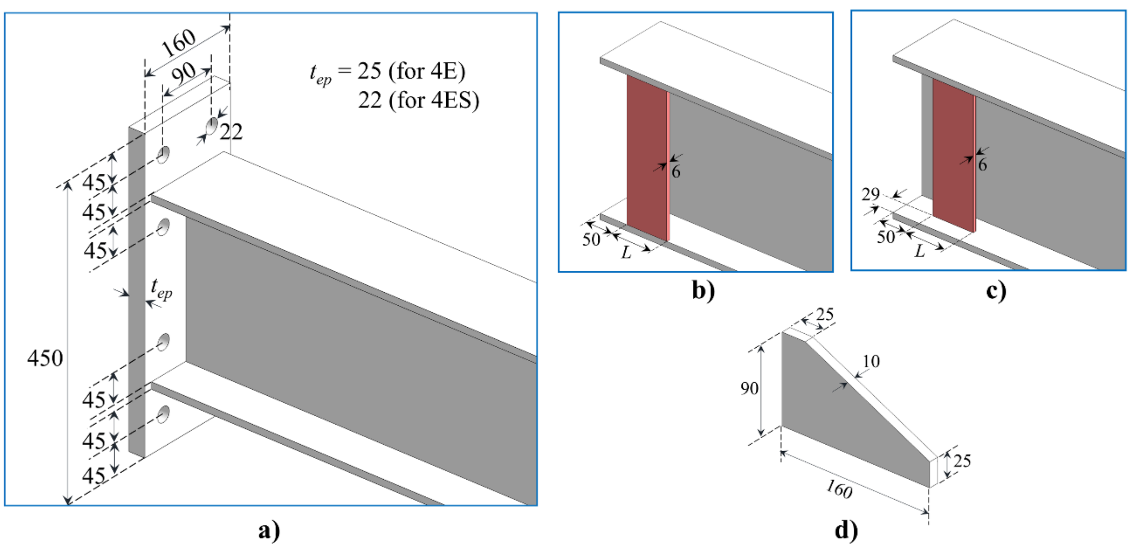

Fig. 2. The dimensions of the beam-to-column connections: (a) end plate dimensions and bolt-hole distances; (b) longitudinal plate dimensions for 4ELP75-O and 4ELP150-O; (c) longitudinal plate dimensions for 4ELP75-N and 4ELP150-N; (d) end plate stiffener dimensions for 4ES.

Table 1. The modeled and analyzed connection configurations.

Model name	Explanation	Geometric view
4E	Four-bolt unstiffened extended end plate connection.	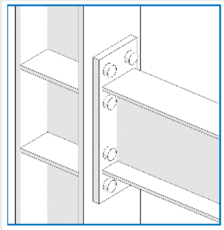
4ELP75-N	Model strengthened with a 75 mm longitudinal plate placed parallel to the beam web and welded to the middle portions of the beam flanges.	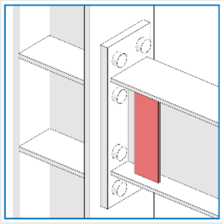
4ELP75-O	Model strengthened with a 75 mm longitudinal plate placed parallel to the beam web and welded to the end portions of the beam flanges.	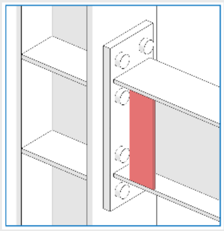
4ELP150-N	Model strengthened with a 150 mm longitudinal plate placed parallel to the beam web and welded to the middle portions of the beam flanges.	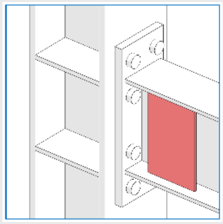
4ELP150-O	Model strengthened with a 150 mm longitudinal plate placed parallel to the beam web and welded to the end portions of the beam flanges.	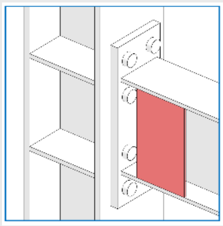
4ES	Four-bolt stiffened extended end plate connection.	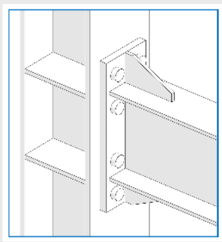

2.2. Loading protocol

The cyclic response of the connection models was investigated using a quasi-static, displacement-controlled loading protocol applied at the beam loading point, as illustrated in Fig. 3. The cyclic displacement history was defined according to the AISC 341-16 seismic loading protocol (AISC 2016), and loading was continued up to a maximum story drift angle of 0.06 rad, corresponding to approximately 6% drift.

The analysis was conducted in two sequential steps. Initially, a bolt pretension force of 172 kN was applied to the M20 high-strength bolts, in compliance with the minimum pretension requirements specified in ANSI/AISC 360-22 (AISC 2022b). Subsequently, reversed cyclic vertical displacements were imposed at the beam loading point. This approach allowed the combined effects of bolt pretension and cyclic deformation demands to be captured throughout the nonlinear response of the connection.

The loading history was defined in terms of the story drift angle, θ (rad), which is calculated using Eq. (1).

$$\theta = \frac{\Delta_{CL}}{L_{CL}} \quad (1)$$

where Δ_{CL} represents the vertical displacement at the beam loading point, and L_{CL} denotes the distance from the loading point to the column centerline. Therefore, the target displacement values for the analyses were determined by multiplying the prescribed drift angle by L_{CL}.

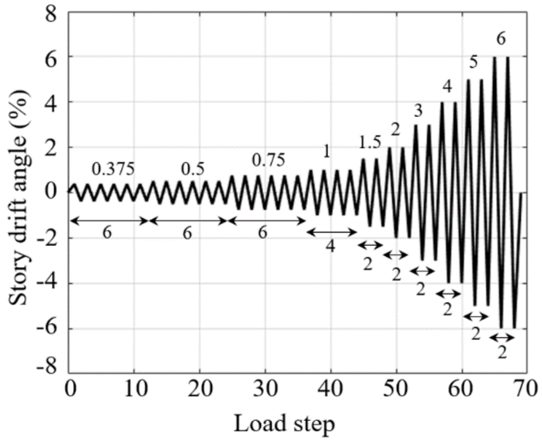

Fig. 3. Cyclic loading history.

2.3. Material properties

In the finite element models, material nonlinearity was addressed by implementing the von Mises yield criterion together with a kinematic hardening rule. The steel components were modeled using multi-linear true stress (σ_{true})-true strain (ε_{true}) relationships to accurately represent the inelastic behavior of beam-to-column connections subjected to cyclic loading. The material properties and corresponding true stress-strain values, as detailed in Table 2, were taken from the study of Gerami et al. (2011). In Table 2, for each material, the first point corresponds to the onset of yielding and the final point to the ultimate stress, while the intermediate points define the strain-hardening response. The elastic modulus (E) of each steel was obtained as the initial slope of its true stress–strain curve in Table 2, giving values between $2.03{\times}10^5$ and $2.06{\times}10^5$ MPa. The multilinear kinematic hardening model in Ansys was defined using the plastic strain (ε_{pl}), listed in the last column of Table 2, obtained as $\varepsilon_{pl} = \varepsilon_{true} - \sigma_{true}/E$. The first point of each curve corresponds to zero plastic strain at the yield stress. A constant Poisson's ratio of 0.3 was used for all materials. This modeling approach allowed the simulations to capture the onset of yielding, subsequent strain hardening, and the development of inelastic regions within the connection zone during cyclic loading.

Table 2. True stress, true total strain, and plastic strain values used in the multilinear kinematic-hardening material model (Gerami et al. 2011).

Material	Component	True stress (MPa)	True total strain	Plastic strain
ASTM A490	Bolt	794	0.003860	0
		1035	0.013500	0.008468
		1035	0.030900	0.025868
		1048	0.200000	0.194905
ASTM A36	End plate	262	0.001276	0
		262	0.014030	0.012754
		476	0.153000	0.150682
ASTM A572 Grade 50	All other components	361	0.001780	0
		361	0.019600	0.017820
		488	0.213400	0.210994

2.4. Element type and mesh

All steel components of the connection, including the beam, column, end plate, stiffener plate, longitudinal plates, and bolts, were discretized using 20-node three-dimensional solid elements (SOLID186). This element type was selected due to its capability to accurately capture material nonlinearity, large deformations, and complex stress distributions in beam-to-column connections. A structured meshing approach was implemented, with mesh refinement applied in regions anticipated to experience high stress gradients and localized inelastic deformations, such as the end plate, bolt region, beam flange adjacent to the connection, panel zone, stiffener plate, and longitudinal plates. In the beam and column regions distant from the joint, where stress variation is less significant, a coarser mesh was utilized to improve computational efficiency without compromising accuracy. The finite element mesh configuration used in the analyses is presented in Fig. 4.

2.5. Contacts

In the finite element models, the interactions between connected components were represented by contact pairs, with the contact behavior defined as either linear-bonded or nonlinear-frictional according to the anticipated interface response. The corresponding contact element formulations were generated automatically by the program according to the geometry and meshing of each contact region, comprising surface-to-surface contact elements (CONTA174) and target elements (TARGE170). The surface-to-surface contact formulation is appropriate for bolted end plate connections, as it represents the separation, finite sliding, and frictional contact-pressure transfer that occur at the end plate, column flange, and bolt interfaces. Nonlinear-frictional contact pairs were defined between the end plate and column flange, end plate and bolt shank, column flange and bolt shank, bolt head and end plate, and nut and column flange. For all frictional interfaces, a coefficient of friction of 0.4 was adopted, representing an average value between the 0.30 (Class A) and 0.50 (Class B) coefficients specified in AISC 360-22 (AISC 2022b). All other interfaces were modeled as linear bonded contacts to prevent relative displacement and to maintain full compatibility in both normal and tangential directions.

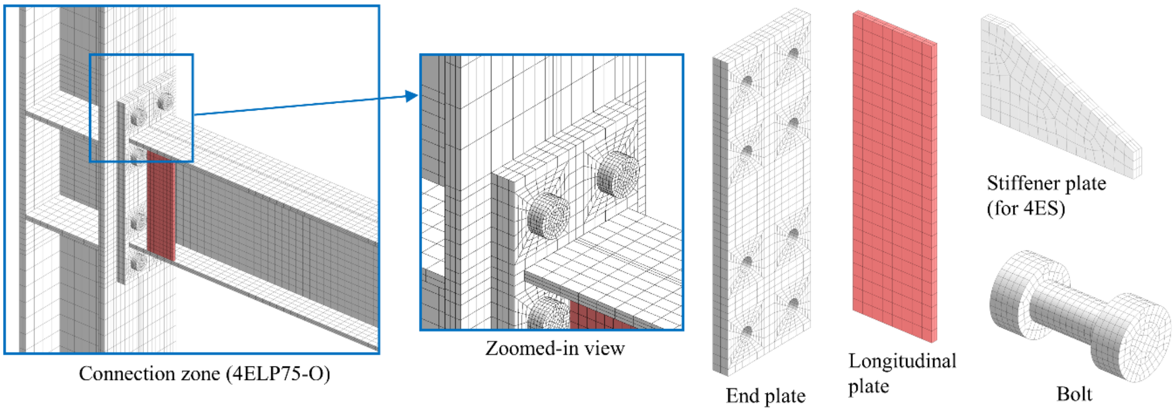

Fig. 4. Mesh of the models.

2.6. Evaluation of the response quantities

The response quantities were obtained from the FE analysis results by post-processing as described below.

2.6.1. Moment

The moment was obtained by multiplying the reaction force at the beam loading point by the distance from the loading point to the column face.

2.6.2. Story drift angle

The story drift angle was obtained from the vertical displacement measured at the beam loading point, divided by the distance from the loading point to the column centerline, in accordance with the definition given in Eq. (1) in Section 2.2.

2.6.3. Dissipated energy

The dissipated energy in the models was determined from the strain energy results of the analysis, evaluated separately for each component, including the beam, column, end plate, continuity plates, bolts, longitudinal plates, and stiffener. For each component, the strain energy was summed over all elements, and the total dissipated energy was calculated as the sum of these component contributions. The strain energy comprises both a recoverable elastic part and the energy dissipated through plastic deformation; at the drift levels examined, the response was dominated by plastic deformation, so that the strain energy predominantly reflects the dissipated energy. To confirm the strain-energy-based values, they were independently checked against the work done by the applied force, obtained by trapezoidal integration of the force–displacement response, and close agreement was obtained, with differences of approximately 1.5% or less. The accumulated strain energy increased monotonically with ongoing plastic deformation. The cumulative dissipated energy at a specific drift level was obtained at the end of the final cycle for that amplitude, with repeated cycles incorporated throughout the loading history.

2.6.4. Bolt force

The axial force in the bolts was determined by measuring the reaction force at the center of each monitored bolt along the axis of the bolt. Two representative bolts were selected for monitoring: Bolt-1, located above the beam flange, and Bolt-2, located between the flanges. It should be noted that, due to the initial pretension applied to the bolts, the axial force in each bolt remained positive throughout the entire loading history. Therefore, the recorded force histories indicate cyclic variations around the pretension force rather than full tension–compression cycles.

2.6.5. Equivalent viscous damping ratio

The energy dissipation efficiency was evaluated using the hysteretic equivalent viscous damping ratio (ξ_{hyst}), computed for each drift amplitude from the moment–story drift response according to Eq. (2):

$$\xi_{hyst} = \frac{E_D}{4\pi E_S} = \frac{E_D}{2\pi M_{\max}\theta_{\max}} \tag{2}$$

Here, E_D is the energy dissipated in a full cycle, E_S is the corresponding stored elastic energy taken as

$\frac{1}{2}M_{\max}\theta_{\max}$, $\theta_{\max}$ is the peak story drift angle of the cycle, and $M_{\max}$ is the moment corresponding to $\theta_{\max}$. The damping ratio was evaluated only for the 3–6% drift levels, each of which consists of two cycles in the AISC protocol and was computed for the second of these two cycles. The dissipated energy E_D was obtained directly from the total strain energy of the complete model, summed over all components of the connection, as its increment over this cycle, taken between two instants one full cycle apart at the same peak-displacement state, so that the recoverable elastic strain energy canceled and only the energy dissipated during the cycle remained. The peak drift $\theta_{\max}$ and the corresponding moment $M_{\max}$ were evaluated at the same instant, taken as the final peak of the selected cycle. Because the applied displacement protocol was symmetric, the positive and negative peaks of a cycle corresponded to the same drift amplitude. Although a minor asymmetry developed between the positive and negative peaks at large drift amplitudes, the same peak was used consistently for all models, so that $M_{\max}$ represents the moment attained at that peak.

2.7. Finite element model validation

To verify the reliability of the developed finite element modeling approach, an additional validation was conducted using the experimentally tested EEP 2 specimen as reported by Morrison and Suarez (2022). In the present validation model, all geometric details, material properties, loading protocol, bolt pretension, and boundary conditions were defined to match those of the reference experimental study (Morrison and Suarez 2022). The EEP 2 specimen comprised an unstiffened eight-bolt extended end plate connection, utilizing a W690×140 beam, a W360×382 column, a 38.1 mm thick end plate, and 31.8 mm diameter ASTM Grade A490 bolts, each pretensioned to 340 kN. Both the beam and column were fabricated from ASTM A992 steel, while the end plate was specified as ASTM A572 Grade 50. The AISC 341-16 loading protocol was applied at the beam tip. The finite element mesh for the EEP 2 specimen is illustrated in Fig. 5.

Fig. 6 presents a comparison of the experimental and numerical moment–story drift responses for the EEP 2 specimen. The finite element model reasonably reproduces the global cyclic behavior, capturing the initial stiffness, the overall shape of the hysteresis loops, the peak moment capacity, and the progressive strength degradation at increased drift amplitudes. While minor discrepancies are observed in certain loading branches, particularly at higher drift levels, the overall correspondence between the experimental and numerical results confirms that the adopted modeling assumptions yield a realistic representation of the connection response.

A qualitative comparison of the damage patterns is provided in Fig. 7, where the experimentally observed failure mode is evaluated against the equivalent plastic strain distribution predicted by the finite element model. Experimentally, yielding initiated in the beam flange and web adjacent to the connection, progressing to local buckling within the beam plastic hinge region, while the column remained essentially elastic throughout the loading protocol. The numerical model successfully captures this sequence, predicting concentrated inelastic deformation and local instability at the beam end. Although there are minor differences in the precise extent and location of local buckling, the overall deformation pattern and the beam-dominated failure mechanism are represented accurately.

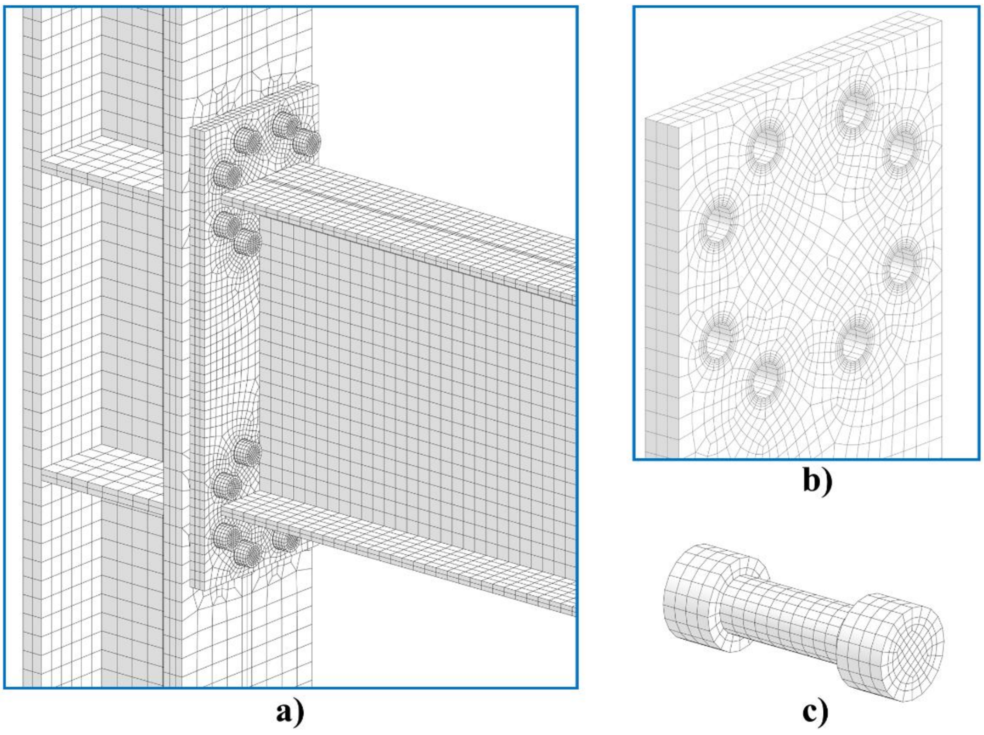

Fig. 5. The finite element mesh of the EEP 2 specimen: (a) Connection region; (b) End plate; (c) Bolt.

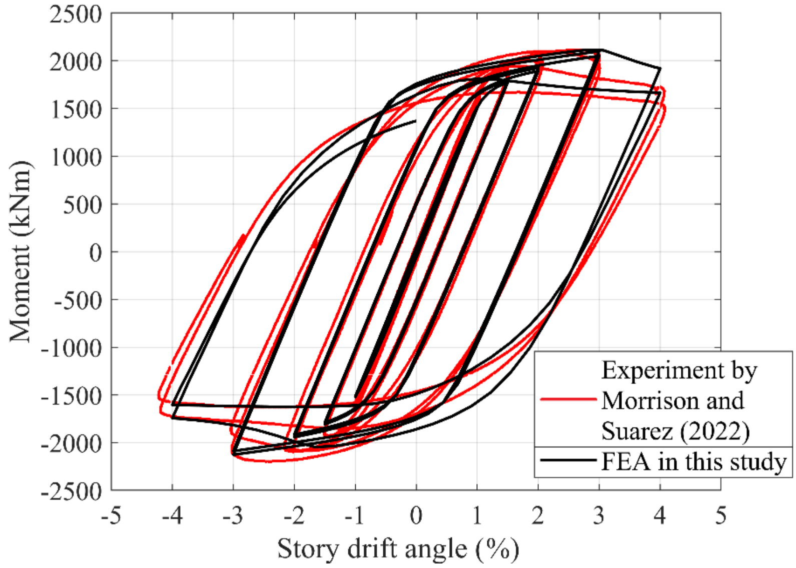

Fig. 6. Comparison of experimental (Morrison and Suarez 2022) and numerical moment-story drift hysteresis curves for the EEP 2 specimen.

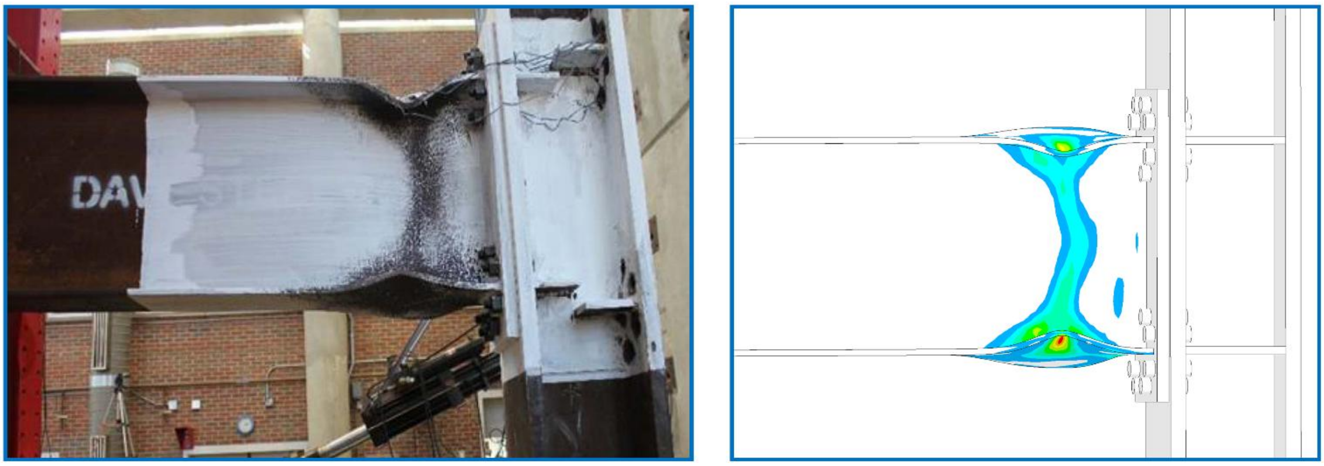

Fig. 7. Comparison of the experimentally observed damage pattern (Morrison and Suarez 2022) and the equivalent plastic strain distribution predicted by the finite element model for the EEP 2 specimen.

The validation results demonstrate that the adopted finite element model is capable of reproducing both the global cyclic response and the local deformation characteristics of the benchmark specimen with acceptable accuracy. Based on these findings, the model was considered appropriate for use in the subsequent parametric investigation of the proposed longitudinal-plate-strengthened end plate connections.

3. Results and Discussion

3.1. Global hysteretic response of the connections

The global cyclic behavior of the beam-to-column connection models was assessed based on the moment–story drift hysteresis curves obtained from nonlinear finite element analyses, as presented in Fig. 8. The comparison includes the unstiffened reference model (4E), four models strengthened with longitudinal plates, and the stiffened model (4ES).

According to ANSI/AISC 341-16, beam-to-column connections in special moment frames (SMFs) are required to sustain a story drift angle of at least 0.04 rad, while maintaining a flexural resistance at the column face of no less than $0.80M_p$ of the connected beam. As shown in Fig. 8, all connections evaluated in this numerical study maintained a flexural moment greater than $0.80M_p$ at a story drift angle of 0.04 rad. Therefore, within the scope of the numerical assessment, the models satisfied the ANSI/AISC 341-16 strength–rotation acceptance limit considered in this study.

The corresponding peak moment values and normalized capacities for all models are summarized in Table 3. The longitudinal-plate models attained higher peak moments than the reference model 4E, with increases ranging from approximately 1.31% to 5.63%, while the stiffened model 4ES reached an increase of approximately 4.49% over 4E.

As illustrated in Fig. 8(a), the reference model 4E exhibits stable and nearly symmetric hysteresis loops at low and moderate drift amplitudes. At larger drift amplitudes, its moment capacity decreases after reaching the peak, approaching $0.80M_p$ at 6% drift, although the connection still satisfies the $0.80M_p$ requirement at 4% drift specified for SMFs. Among the six models, 4E develops the lowest moment capacity.

The addition of longitudinal plates results in a notable improvement in the global hysteretic response. As shown in Figs. 8(b-c), both 4ELP75-N and 4ELP75-O develop higher moment capacities than the reference model 4E across nearly the entire drift range, while maintaining stable and full hysteresis loops up to large drift amplitudes. Between these two configurations, 4ELP75-N sustains slightly higher moment resistance at higher drift amplitudes.

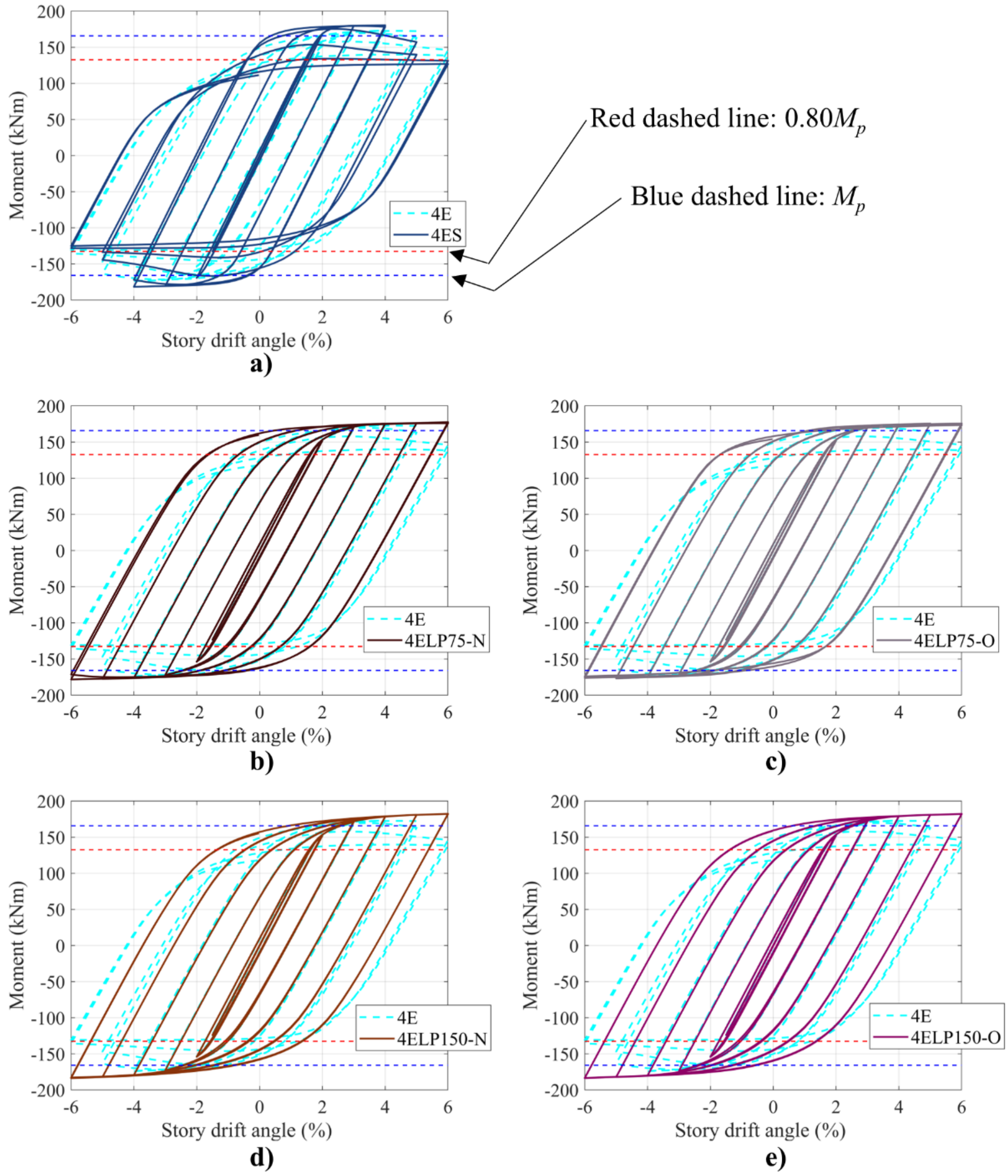

Fig. 8. Comparison of moment–story drift hysteresis responses: (a) 4E and 4ES; (b) 4E and 4ELP75-N; (c) 4E and 4ELP75-O; (d) 4E and 4ELP150-N; (e) 4E and 4ELP150-O.

Table 3. Summary of the peak flexural response of the connection models.

Model	M_{max} (kNm)	M_{max}/M_p	M/M_p at 4% drift	Increase in M_{max} relative to 4E (%)
4E	173.81	1.045	1.045	-
4ELP75-N	178.25	1.072	1.060	2.55
4ELP75-O	176.08	1.060	1.053	1.31
4ELP150-N	183.60	1.104	1.079	5.63
4ELP150-O	183.54	1.104	1.082	5.60
4ES	181.62	1.092	1.092	4.49

Further improvement is achieved by increasing the longitudinal plate length to 150 mm. As presented in Fig. 8(d-e), both 4ELP150-N and 4ELP150-O display the most stable hysteresis loops and the highest moment capacities among the longitudinal-plate-strengthened models. Comparison of the 75 mm and 150 mm plate configurations indicates that plate length has a greater effect on the hysteretic response than plate location. The difference between the N and O placements is relatively minor, with the N configuration performing slightly better for the 75 mm plates, while both 150 mm configurations show similar behavior.

The stiffened model 4ES, as shown in Fig. 8(a), also achieves a significant increase in strength compared to 4E. However, its hysteretic response differs from that of the longitudinal-plate-strengthened models. Although 4ES attains high moment levels at moderate drift amplitudes, loop distortion and response asymmetry are observed at larger drift cycles. The deterioration in loop stability is more evident than in the 150 mm longitudinal plate configurations. These results indicate that while the conventional stiffener is effective in increasing connection strength, it does not provide the same level of cyclic stability as longitudinal plate strengthening under severe drift demands.

In summary, the results presented in Fig. 8 show that both strengthening strategies enhance the hysteretic performance of the unstiffened reference connection. The longitudinal plate configurations, in particular, provide a more balanced improvement in strength and loop stability. The 150 mm longitudinal plates yield the most favorable global response, indicating that increasing plate length is an effective approach for improving the seismic performance of bolted extended end plate connections.

3.2. Energy dissipation capacity

The cumulative dissipated energy of the connection models at story drift angles ranging from 3% to 6% is presented in Fig. 9. In this assessment, the individual contributions of the beam, column, end plate, continuity plates, bolts, longitudinal plates, and stiffener were quantified to determine the distribution of inelastic demand within the connection region. The contributions of the beam, column, and end plate, which together accounted for nearly the entire dissipated energy, are summarized in Table 4 for the 4% and 6% drift levels.

At 4% drift, the total dissipated energy of the longitudinal-plate models was comparable to that of the reference model 4E (34.95 kNm), ranging from 33.76 to 34.75 kNm, while the stiffened model 4ES reached a higher value of 41.09 kNm. At 6% drift, the total dissipated energy of all configurations remained within a narrow range of 114.53 to 119.58 kNm. The longitudinal-plate models exceeded the reference model 4E by approximately 2.2% to 4.4%, and the stiffened model 4ES by approximately 4.0%, confirming that the total energy dissipation was comparable across all configurations and that the principal effect of the strengthening details was a change in the distribution of the dissipated energy rather than a significant increase in its total magnitude.

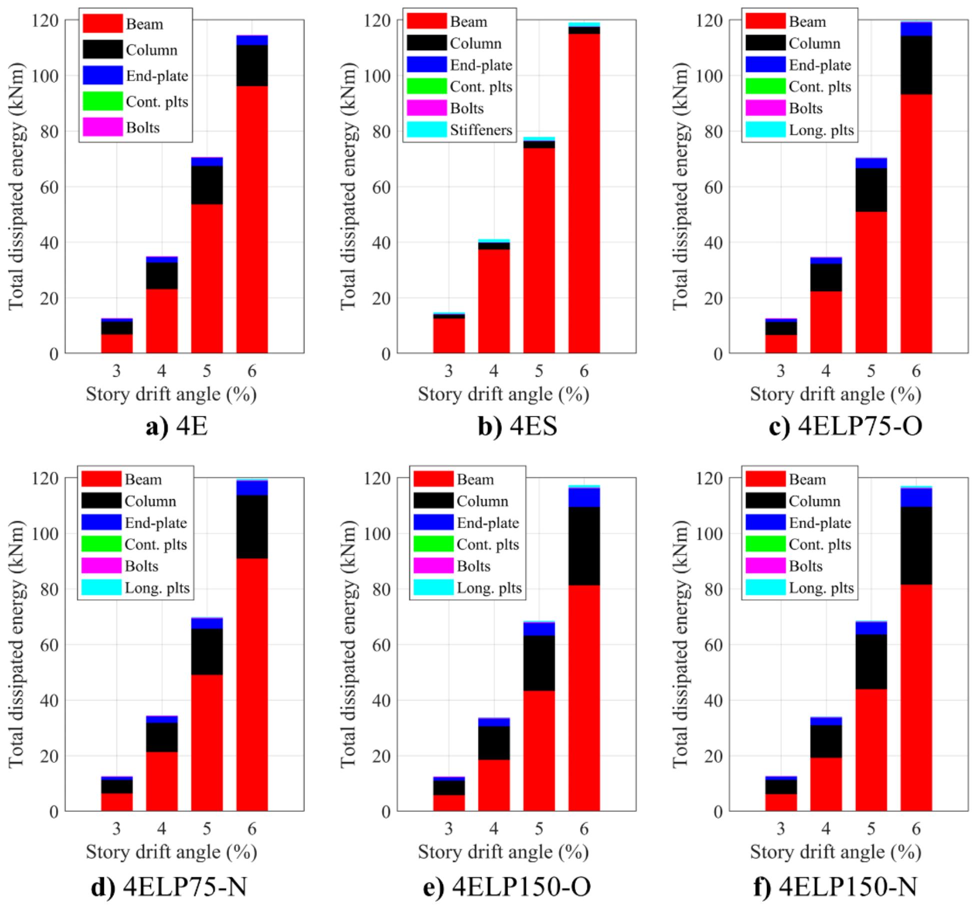

Fig. 9. Comparison of cumulative dissipated energy components versus story drift angle.

Table 4. Summary of the energy dissipation of the connection models.

Model	Total dissipated energy at 4% drift (kNm)	Total dissipated energy at 6% drift (kNm)	Energy dissipation contributions at 4% drift (%)			Energy dissipation contributions at 6% drift (%)		
			Beam	Column	End plate	Beam	Column	End plate
4E	34.95	114.53	66.2	27.3	5.8	83.9	13.0	3.0
4ELP75-N	34.47	119.58	61.9	30.5	6.6	76.0	19.1	4.2
4ELP75-O	34.75	119.57	64.1	28.7	6.3	77.9	17.6	4.0
4ELP150-N	34.03	117.04	56.5	34.6	7.6	69.6	24.0	5.5
4ELP150-O	33.76	117.34	54.8	35.8	8.1	69.3	24.0	5.7
4ES	41.09	119.08	90.8	5.9	0.2	96.5	2.1	0.1

In the reference model 4E, the dissipated energy at 6% drift was concentrated in the beam, which accounted for 83.9% of the total, while the column and end plate contributed 13.0% and 3.0%, respectively. The addition of longitudinal plates progressively shifted the inelastic demand from the beam toward the column and end plate, and this shift became more pronounced as the plate length increased. For the 75 mm models, the beam share decreased to 76.0% (4ELP75-N) and 77.9% (4ELP75-O), with the column contribution rising to 19.1% and 17.6%, respectively. For the 150 mm models, the beam share decreased further to 69.6% (4ELP150-N) and 69.3% (4ELP150-O), while the column contribution increased to 24.0% in both cases and the end plate contribution to 5.5% and 5.7%. The effect of plate location was minor and diminished with plate length, as the two 150 mm configurations exhibited nearly identical distributions. It is also noted that the direct energy contribution of the longitudinal plates themselves remained negligible; their role was therefore to redistribute the inelastic demand toward the column and end plate rather than to dissipate a significant portion of the energy directly.

In contrast, the stiffened model 4ES exhibited the opposite trend, with the dissipated energy becoming even more concentrated in the beam, which accounted for 96.5% of the total at 6% drift, while the column and end plate contributions reduced to 2.1% and 0.1%, respectively. As with the longitudinal plates, the direct energy contribution of the stiffener itself was negligible. This indicates that the conventional stiffener enhances the dissipation capacity primarily by promoting plastic deformation in the beam, whereas the longitudinal plates achieve a more distributed inelastic response by engaging the column and end plate. For all models, the beam share increased between 4% and 6% drift, reflecting the increasing dominance of beam plasticity at larger drift demands. According to the strong-column weak-beam principle, energy dissipation in moment-resisting frames should be concentrated in the beam to maintain the intended seismic hierarchy; therefore, the redistribution observed in the longitudinal-plate models, which was most pronounced for the 150 mm configurations with the column share increasing from 13.0% in 4E to 24.0%, underlines the importance of verifying through component capacity checks that the column and end plate demands remain within acceptable limits.

3.3. Distribution of bolt forces

The distribution of axial force within the tension bolt group was assessed based on the bolt force versus story drift relationships for two representative bolts, as illustrated in Fig. 10.

In the reference model (4E), both bolts display stable cyclic force histories, with axial force increasing as the bolt group is engaged in tension. At higher drift amplitudes, Bolt-1 develops slightly greater axial force than Bolt-2. During load reversal, both bolts unload toward the pretension level. The axial force in Bolt-1 increased by approximately 72 kN and approximately 64 kN in Bolt-2, relative to the initial pretension of 172 kN.

For the 75 mm longitudinal-plate models (4ELP75-O and 4ELP75-N), a modest increase in peak bolt force is observed relative to the reference model 4E. In both configurations, Bolt-1 continues to attract slightly higher force than Bolt-2, and the cyclic force histories remain smooth and stable. The peak force in Bolt-1 increased by approximately 78 kN (4ELP75-N) and 76 kN (4ELP75-O), corresponding to increases of approximately 6–8% over 4E. The difference between the O and N plate placements is minimal, and no significant variation in bolt force distribution is evident at this plate length.

A more pronounced change is evident in the 150 mm longitudinal-plate models (4ELP150-O and 4ELP150-N). In these cases, the peak axial forces exceed those observed in both the reference model and the 75 mm plate configurations, particularly for Bolt-1. The force excursion during load reversal is also more significant, with Bolt-1 experiencing a greater reduction in axial force before increasing again under the opposite loading phase. The peak force in Bolt-1 increased by approximately 83 kN (for both 4ELP150-O and 4ELP150-N), representing increases of approximately 15% relative to 4E, accompanied by a wider cyclic force range. These findings indicate that increasing the plate length intensifies the engagement of the monitored bolts and accentuates the difference between the outer and inner bolts, rather than achieving a more uniform force distribution. The resulting increase in tensile demand on the bolts is a critical consideration for design. If the bolts are not adequately sized for this localized force increase, the failure mode may shift from ductile beam flexural yielding to brittle bolt fracture or thread stripping. The effect of plate placement remains secondary, as both 4ELP150-O and 4ELP150-N show similar trends.

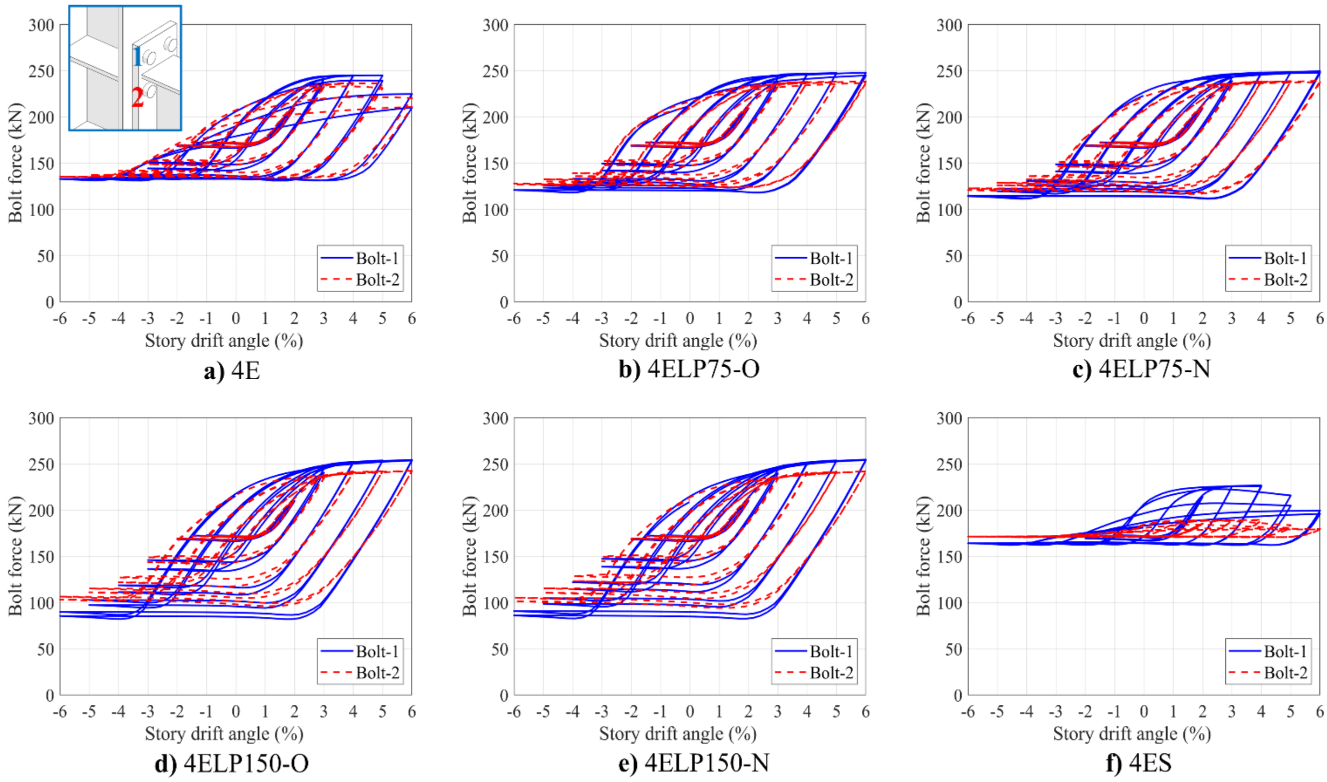

Fig. 10. Variation of bolt axial forces with story drift angle under cyclic loading for different connection configurations: (a) 4E; (b) 4ELP75-O; (c) 4ELP75-N; (d) 4ELP150-O; (e) 4ELP150-N; (f) 4ES.

The stiffened model (4ES) demonstrates a distinctly different bolt force response. The variation in Bolt-2 remains limited throughout the loading history, and the increase in Bolt-1 is also substantially smaller than in the longitudinal-plate-strengthened models. In contrast, the stiffened model 4ES exhibited the lowest bolt demand, with the peak force in Bolt-1 increasing by approximately 55 kN, which is approximately 24% lower than the corresponding increase in 4E. As a result, the bolt force loops are considerably narrower compared to those of 4E and the longitudinal-plate configurations. This behavior indicates that the stiffener modifies the internal force-transfer mechanism and reduces the tensile demand on the monitored bolt pair, especially on the inner bolt.

Fig. 10 shows that longitudinal plate strengthening, particularly with a plate length of 150 mm, increases the tensile demand on the monitored bolts and accentuates the difference between Bolt-1 and Bolt-2. In contrast, the stiffened configuration (4ES) limits the cyclic variation of bolt forces and maintains a lower level of bolt demand. These results demonstrate that longitudinal plate and stiffener strengthening strategies enhance connection behavior through different internal mechanisms.

3.4. Potential failure mechanisms

The potential failure mechanisms of the connection models were evaluated based on equivalent plastic strain (von Mises) contours at the end of the cyclic analyses, as shown in Fig. 11. These contours indicate the intensity and distribution of inelastic deformation in the joint region, allowing assessment of how strengthening details influence the governing failure mode.

In the reference model (4E), shown in Fig. 11(a), plastic strain is concentrated in the beam flange and web near the end plate. The highest strain occurs close to the connection face, indicating that inelastic deformation is localized within a short region adjacent to the end plate. This pattern corresponds to the formation of a plastic hinge at or near the beam-to-column interface.

The longitudinal-plate-strengthened models show a different deformation pattern. In both 75 mm configurations (4ELP75-O and 4ELP75-N), plastic strain near the connection face is reduced compared to 4E, and inelastic deformation is distributed over a wider area of the beam flange and web. Some plastic strain develops in the longitudinal plates, mainly near their ends, indicating their role in redistributing internal forces. Among the 75 mm models, 4ELP75-N has a lower maximum plastic strain than 4ELP75-O.

A similar but more favorable trend is seen in the 150 mm longitudinal-plate models. As shown in Fig. 11(d) and (e), both 4ELP150-O and 4ELP150-N have lower peak plastic strain than the reference model (4E) and show a more distributed inelastic response along the beam flange. The concentration of plastic deformation near the end plate is less severe, and the yielded zone extends farther from the column face. Increasing the plate length improves redistribution of inelastic demand and reduces strain localization at the beam end. Among all longitudinal-plate configurations, 4ELP150-O has the lowest maximum plastic strain, while 4ELP150-N is similar to 4ELP75-N. The results indicate that both plate length and placement influence strain redistribution, and optimal placement depends on plate length.

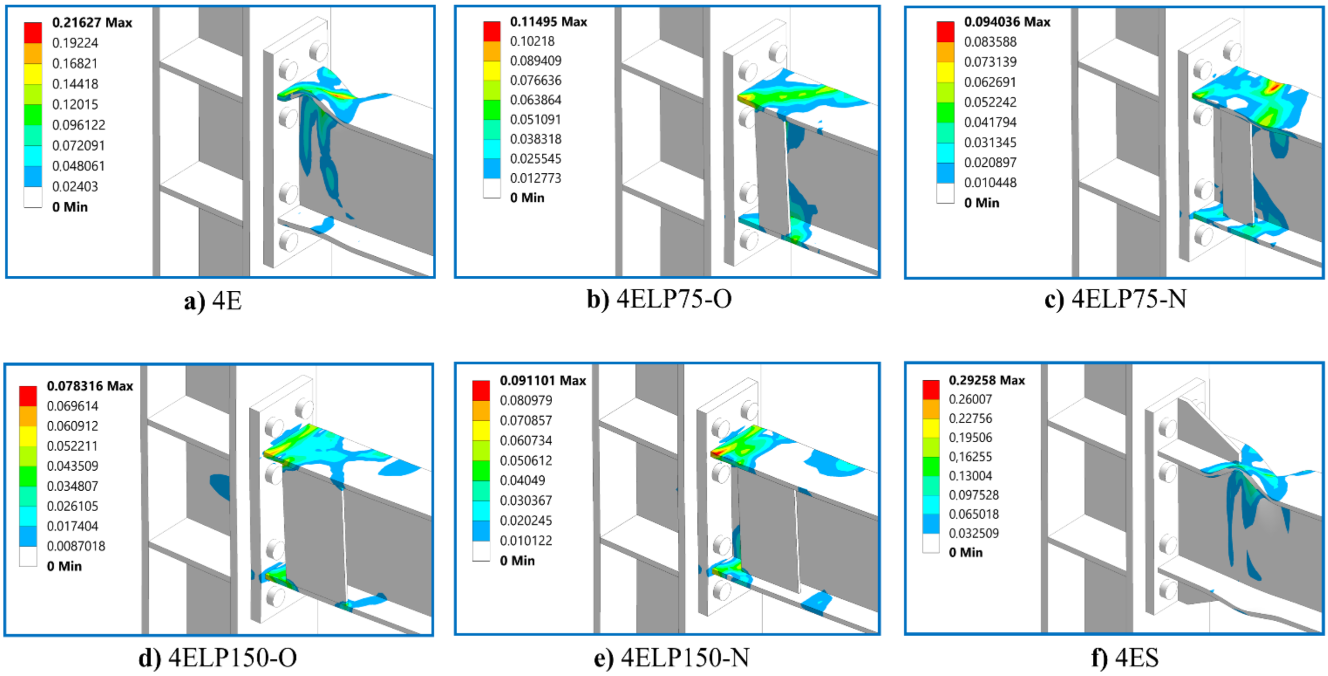

Fig. 11. Plastic strain distribution and dominant deformation patterns in the beam–column connection region for different configurations: (a) 4E; (b) 4ELP75-O; (c) 4ELP75-N; (d) 4ELP150-O; (e) 4ELP150-N; (f) 4ES.

The stiffened model (4ES), shown in Fig. 11(f), has the most severe strain concentration among all models. The highest equivalent plastic strain occurs in the beam flange near the stiffener-beam junction and in the adjacent beam web. This shows that the conventional stiffener moves the plastic hinge away from the column face and weld root, but also increases strain localization at the beam end. Conversely, it is important to ensure that the longitudinal plates do not over-strengthen the beam section, which could shift yielding into the connection elements or the column panel zone.

The maximum equivalent plastic strain in the reference model 4E was found to be approximately 0.216. For the models with 75 mm longitudinal plates, the maximum equivalent plastic strain decreased to approximately 0.115 for 4ELP75-O and 0.094 for 4ELP75-N, which corresponds to reductions of about 47% and 56% compared to 4E. The models with 150 mm longitudinal plates showed the lowest maximum plastic strain values, with approximately 0.078 for 4ELP150-O and 0.091 for 4ELP150-N, representing reductions of about 64% and 58% compared to 4E. On the other hand, the stiffened model 4ES exhibited the highest maximum equivalent plastic strain, reaching approximately 0.293, which is an increase of about 36% relative to 4E. This result is consistent with the most pronounced strain localization observed among all the configurations.

Overall, Fig. 11 shows that longitudinal plate strengthening reduces peak plastic strain in the beam-end region and promotes a more distributed inelastic deformation pattern, especially in the 150 mm configurations. In contrast, the stiffened configuration (4ES) results in the highest local strain demand and the most concentrated failure mechanism. These results indicate that longitudinal plates are more effective than the conventional stiffener in reducing severe strain localization at the connection region.

3.5. Hysteretic equivalent viscous damping ratio

Variation in the hysteretic equivalent viscous damping ratio (ξ_{hyst}) with story drift angle for all six models is presented in Fig. 12.

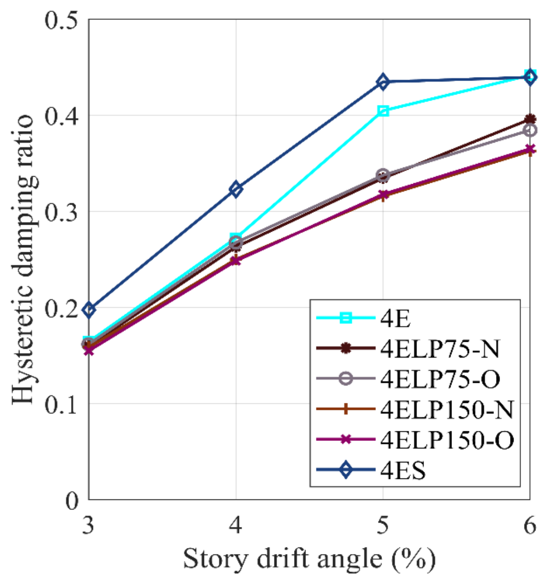

Fig. 12. Variation in the hysteretic equivalent viscous damping ratio with story drift angle for all six models

A consistent increase in ξ_{hyst} was observed for all models as drift demand increased, indicating a greater contribution of inelastic deformation to energy dissipation at higher drift levels. At a drift of 3%, the damping ratios for all configurations were nearly identical, ranging from 0.155 to 0.198. With increasing drift, the stiffened model 4ES demonstrated the highest damping ratio up to 5% drift, reaching 0.323 at 4% and 0.435 at 5%. At 6% drift, both the reference model 4E and the stiffened model 4ES achieved comparable maximum values of 0.442 and 0.440, respectively. The longitudinal-plate models showed lower damping ratios, and this difference became more significant at larger drift amplitudes. At 6% drift, the 75 mm longitudinal-plate models reached 0.396 (4ELP75-N) and 0.385 (4ELP75-O), while the 150 mm models reached 0.363 (4ELP150-N) and 0.365 (4ELP150-O). For the longitudinal-plate models, increasing the plate length resulted in a slight reduction in damping ratio, whereas the effect of plate location was negligible.

The lower damping ratios observed in the longitudinal-plate models are primarily due to their higher moment capacities, rather than a decrease in total energy dissipation. As indicated in Eq. (2), ξ_{hyst} is normalized by the moment corresponding to θ_{max}. The longitudinal-plate models achieved higher moment capacities (see Section 3.1) while dissipating a similar amount of total energy (see Section 3.2), resulting in lower normalized damping ratios. This outcome is consistent with the more distributed and less concentrated plastic deformation observed in these models (Section 3.4), where higher moments were attained with reduced strain localization at the beam end. Therefore, the lower damping ratios in the longitudinal-plate models reflect their increased moment capacity, not a deficiency in hysteretic performance, since ξ_{hyst} represents the dissipated energy relative to the attained moment. In contrast, the stiffened model 4ES reached its high damping ratio through concentrated and intense plastic deformation in the beam, which is consistent with the highest peak plastic strain among all models (Section 3.4). All configurations, including the longitudinal-plate models, maintained high equivalent viscous damping ratios above 0.36 at 6% drift, demonstrating substantial hysteretic energy dissipation in all cases.

3.6. Component capacity verification

The redistribution of inelastic demand toward the column and end plate regions, as identified in Section 3.2, was evaluated by performing component capacity checks to assess whether the intended yielding hierarchy and component capacity limits were maintained. These checks used the moment delivered to the column face, which was taken as the peak moment from each model as shown in Table 3, along with the panel zone shear forces and peak bolt forces obtained directly from the FE models.

The strong-column weak-beam requirement was evaluated in accordance with ANSI/AISC 341-16, which requires the ratio of the sum of the column plastic flexural strengths to the sum of the beam probable flexural strengths projected to the column centerline to exceed unity. The sum of the column plastic flexural strengths above and below the joint, evaluated as $2\times Z_cF_y$ with the column axial force neglected, was 733.5 kNm. The sum of the beam flexural strengths projected to the column centerline was determined according to Eq. (3):

$$\sum M_{pb} = \sum(M_{pr} + \alpha_s M_v) \tag{3}$$

where M_{pr} is the probable maximum moment at the plastic hinge, α_s is the force level adjustment factor taken as 1.0 for load and resistance factor design, and M_v is the additional moment due to shear amplification from the plastic hinge location to the column centerline. The probable beam flexural strength was determined according to Eq. (4):

$$M_{pr} = C_{pr}R_yF_yZ_b \tag{4}$$

Here, $C_{pr} = (F_y + F_u)/(2F_y) \leq 1.2$ is the peak connection strength factor, R_y is the ratio of expected to specified minimum yield strength, and Z_b is the plastic section modulus of the beam. For the ASTM A572 Grade 50 beam, C_{pr} was taken as 1.18 and R_y as 1.1, resulting in a probable beam moment (M_{pr}) of 215.0 kNm. With the shear amplification moment included, ΣM_{pb} is 233.5 kNm, giving a column-to-beam flexural strength ratio of 3.1 for all configurations. This result confirms that the column remained elastic in flexure, no column flexural hinge formed, and the redistribution of dissipated energy toward the column did not affect the intended yielding hierarchy.

The column energy contribution was associated with shear deformation of the panel zone. The panel zone shear force was obtained directly from the FE models as the resultant horizontal force on a section through the mid-height of the panel zone, and the resulting demand-to-capacity ratios are summarized in Table 5. The available panel zone shear strength of the HE240B column was determined according to Eq. (5):

$$R_v = 0.60F_yd_ct_{wc}\left[1 + \frac{3b_{fc}t_{fc}^2}{d_bd_ct_{wc}}\right] \tag{5}$$

where d_c and t_{wc} are the depth and web thickness of the column, b_{fc} and t_{fc} are the width and thickness of the column flange, and d_b is the beam depth. This formulation includes the contribution of the column flanges mobilized during inelastic deformation of the panel zone, resulting in an available strength of 687 kN. For all configurations, the panel zone shear demand remained within this strength, with demand-to-capacity ratios between 0.71 and 0.82. The panel zone shear force increased in line with the column energy contribution reported in Section 3.2, from 490 kN for the stiffened model (4ES), which had the lowest column energy share and ratio of 0.71, to 567 kN for the 150 mm configurations, which had the highest. This correspondence shows that the increased column energy participation in the longitudinal-plate models was due to limited panel zone shear yielding, which is an accepted ductile mechanism under cyclic loading and remained within the available panel zone strength.

Table 5. Panel zone shear demand obtained from the FE models and the corresponding demand-to-capacity ratios.

Model	V_u (kN)	V_u/R_v
4E	540.4	0.79
4ELP75-N	551.5	0.80
4ELP75-O	546.0	0.79
4ELP150-N	566.5	0.82
4ELP150-O	564.9	0.82
4ES	490.4	0.71

The end plate thickness was set at 25 mm according to the thick-plate design provisions of ANSI/AISC 358-22, which are intended to keep the end plate essentially elastic and to concentrate inelastic deformation in the beam. The analyses in Section 3.2 showed that the end plate energy contribution ranged from 3.0% to 5.7%, which aligns with this design approach and confirms that the end plate did not control the connection response.

Bolt tension demand was identified as the governing limit state, as summarized in Table 6. The bolt tensile rupture strength was calculated using Eq. (6):

$$R_n = A_b F_{nt} \tag{6}$$

where A_b is the nominal area of the bolt and F_{nt} is the nominal tensile stress, taken as $0.75F_{ub}$ in accordance with ANSI/AISC 360-22, with F_{ub} the ultimate tensile strength of the bolt material. For the M20 ASTM A490 bolts, A_b is 314 mm^2 and F_{nt} is 786 MPa, resulting in a tensile rupture strength of 247 kN. The peak axial force in the most heavily loaded bolt reached 0.99 of this strength in the reference model 4E, reached or slightly exceeded it in the longitudinal-plate models, with ratios of 1.00 to 1.01 for the 75 mm configurations and 1.03 for the 150 mm configurations, and remained below capacity at 0.92 for the stiffened model 4ES. These results indicate that the M20 ASTM A490 bolts are at or beyond their nominal tensile capacity in the longitudinal-plate configurations, and that a larger bolt diameter or higher grade may be required to develop the strengthened connections without bolt tensile rupture. As the finite element bolt model does not incorporate a fracture criterion, the analysis captures the bolt force demand but not the rupture itself.

Table 6. Peak axial force in the most heavily loaded tension bolt (Bolt-1) and the corresponding demand-to-capacity ratios.

Model	T_u (kN)	T_u/R_n
4E	244	0.99
4ELP75-N	250	1.01
4ELP75-O	248	1.00
4ELP150-N	255	1.03
4ELP150-O	255	1.03
4ES	227	0.92

4. Conclusions

In this study, the cyclic behavior of bolted extended end plate beam-to-column connections strengthened with longitudinal plates parallel to the beam web was investigated through numerical simulation. Six representative connection models were established and analyzed under the AISC cyclic loading protocol. These included an unstiffened reference connection (4E), a stiffened connection (4ES), and four configurations incorporating longitudinal plates. The main conclusions can be summarized as follows:

- The unstiffened reference model (4E) demonstrated stable and nearly symmetric hysteretic behavior at low and moderate drift levels. At larger drift amplitudes, however, it exhibited strength degradation, with the flexural resistance approaching $0.80M_p$ at 6% drift. Among the six models, 4E developed the lowest moment capacity, with its inelastic deformation concentrated in the beam region adjacent to the connection.
- The addition of longitudinal plates enhanced the overall cyclic performance of the connections. All models strengthened with longitudinal plates developed higher moment capacities and exhibited less strength degradation at large drift amplitudes than the reference model (4E).
- Among the parameters investigated, plate length was found to have a more significant effect on connection response than plate location. The configurations with 150 mm longitudinal plates exhibited the most favorable hysteretic behavior, minimal strength degradation, and the most distributed inelastic deformation patterns among the strengthened models.
- The cumulative energy dissipated by the longitudinal-plate-strengthened models was generally comparable to, and at large drift amplitudes slightly exceeded, that of the reference model (4E). The presence of longitudinal plates modified the distribution of dissipated energy by increasing the contribution of the column and end plate regions. The increased column contribution was associated with a higher panel zone shear demand, which component capacity checks confirmed remained within the available panel zone strength and corresponded to limited panel zone yielding.
- The longitudinal plate configurations, particularly those utilizing 150 mm plates, resulted in increased engagement of the monitored bolts and produced higher tensile forces in the bolts compared to the reference model (4E). As a result, the bolt tension demand reached or exceeded the nominal tensile capacity in these configurations, and a larger bolt diameter or higher grade may be required to prevent brittle bolt tensile rupture.
- Analysis of plastic strain contours indicated that the addition of longitudinal plates reduced peak strain demand in the beam-end region and facilitated a more distributed inelastic mechanism. This effect was most pronounced in the models with 150 mm plates. In contrast, the stiffened model (4ES) exhibited the highest local strain concentrations and the most localized failure pattern among all configurations analyzed.
- All configurations maintained high hysteretic equivalent viscous damping, with values above 0.36 at 6% drift. The longitudinal-plate models exhibited slightly lower damping ratios than the reference (4E) and stiffened (4ES) models, reflecting their higher moment capacity rather than a reduction in dissipated energy, since the damping ratio is normalized by the attained moment.

In summary, the findings indicate that longitudinal plates installed parallel to the beam web represent an effective strengthening alternative for bolted extended end plate connections subjected to cyclic loading. Compared to the conventional stiffener detail (4ES), this approach achieves a more favorable balance between strength enhancement and distributed inelastic response, and does not introduce the upward projection characteristic of end plate stiffeners. More specifically, the longitudinal plates reduced the peak plastic strain in the beam-end region and maintained stable hysteretic behavior at large drift amplitudes, in contrast to the conventional stiffener, which produced the highest local strain concentration among all configurations.

5. Limitations and Future Work

Despite the comprehensive numerical findings presented in this study, several limitations should be acknowledged and addressed in future research.

- The conclusions of this study are derived primarily from three-dimensional nonlinear finite element simulations. Although the modeling approach was validated by comparison with the experimental response of the EEP 2 benchmark specimen, the specific longitudinal-plate configurations introduced in this research have not been subjected to dedicated physical testing. Therefore, experimental studies are required to verify the hysteretic behavior, bolt force development, and local failure mechanisms of the proposed details under cyclic loading conditions.
- The scope of the numerical investigation was restricted to a single beam-to-column configuration and a limited set of geometric parameters. The analyses were conducted using one beam section, one column section, a single end plate configuration, and two longitudinal plate lengths at two plate locations. As a result, the conclusions drawn from this study are applicable only within the boundaries of the investigated models. Further research should extend the parametric study to include a wider range of beam and column sizes, end plate thicknesses, bolt diameters, plate thicknesses, steel grades, and weld details to establish more comprehensive design-oriented trends.
- The loading protocol employed in this study was limited to the AISC quasi-static cyclic loading history. Although this protocol is suitable for assessing connection performance under standardized seismic qualification requirements, it does not capture all characteristics of earthquake loading. Specifically, the effects of loading rate, cumulative damage resulting from irregular loading histories, and record-to-record variability were not addressed. Additional research utilizing nonlinear time-history analysis or experimental dynamic loading is necessary to further evaluate the seismic robustness of the proposed strengthening approach.
- The present research was limited to the evaluation of connection-level behavior. The effects of longitudinal plate strengthening on the global response of steel moment-resisting frames, such as inter-story drift demand, force redistribution at the system level, collapse mechanisms, and residual deformations, were not examined. Incorporating the proposed connection details into frame-scale numerical models is necessary to assess their effectiveness within complete structural systems.
- This study did not provide a quantitative evaluation of constructability, retrofit feasibility, fabrication requirements, or cost efficiency. While longitudinal plates may offer geometric and behavioral advantages compared to conventional stiffener details, their practical implementation should be further investigated with respect to welding accessibility, fabrication sequence, inspection requirements, and economic considerations.

Accordingly, future research should prioritize experimental validation of the proposed connection details, expansion of the geometric and material parameter space, assessment under dynamic earthquake loading, and evaluation of frame-level performance and practical applicability. These studies will contribute to the development of design recommendations for longitudinal-plate-strengthened bolted extended end plate connections.

Acknowledgements

None declared.

Funding

The authors received no financial support for the research, authorship, and/or publication of this manuscript.

Conflict of Interest

The authors declare no potential conflicts of interest with respect to the research, authorship, and/or publication of this manuscript.

Data Availability

The datasets generated and/or analyzed during the current study are not publicly available but are available from the corresponding author upon reasonable request.

AI Assistance

During the preparation of this manuscript, Google Gemini 3.1 Pro was used exclusively for language editing and stylistic refinement. The authors take full responsibility for the content, interpretation, and conclusions of the published article.

Author Contributions

All authors made substantial contributions to the conception and design of the study, acquisition of data, analysis and interpretation of data; drafted or critically revised the manuscript for important intellectual content; and approved the final version to be published.

References

Abidelah A, Bouchaïr A, Kerdal DE (2012). Experimental and analytical behavior of bolted end-plate connections with or without stiffeners. *Journal of Constructional Steel Research*, 76, 13–27.

AISC (2016). *Seismic Provisions for Structural Steel Buildings (ANSI/AISC 341-16)*. American Institute of Steel Construction, Chicago, IL, USA.

AISC (2022a). *Prequalified Connections for Special and Intermediate Steel Moment Frames for Seismic Applications (ANSI/AISC 358-22)*. American Institute of Steel Construction, Chicago, IL, USA.

AISC (2022b). *Specification for Structural Steel Buildings (ANSI/AISC 360-22)*. American Institute of Steel Construction, Chicago, IL, USA.

ANSYS (2024). *Ansys Academic Research Mechanical, Release 2024 R2*. ANSYS Inc., Canonsburg, PA, USA.

Bahaari MR, Sherbourne AN (1996). Structural behavior of end-plate bolted connections to stiffened columns. *Journal of Structural Engineering*, 122(8), 926–935.

Bursi OS, Jaspart JP (1998). Basic issues in the finite element simulation of extended end plate connections. *Computers & Structures*, 69(3), 361–382.

Cai M, Liu X, Wang Q, Gu H, Wang P, Liu Y, Liu F (2022). Seismic performance of thread-fixed one-side bolts bolted extended endplate connection to HSST column with internal strengthening components. *Journal of Building Engineering*, 45, 103615.

Couchaux M, Madhouni M (2022). Theoretical models for T-stubs in contact with intermediate layer. *Journal of Constructional Steel Research*, 192, 107158.

El-Sa'eed SA (2024). Strengthening and retrofitting of steel moment connections. In: Abdullah W, Chaudhary MT, Kamal H, Parol J, Almutairi A, editors. *Civil Structural Health Monitoring: Proceedings of CSHM-9 Workshop*. Springer, Cham, Switzerland, pp. 92–104.

Gerami M, Saberi H, Saberi V, Daryan AS (2011). Cyclic behavior of bolted connections with different arrangement of bolts. *Journal of Constructional Steel Research*, 67(4), 690–705.

Ghamari A, Amini SM, De Crescenzo C, Musmarra D (2023). Investigating the behaviour of steel end-plate connections with shape memory alloy bolts. *Proceedings of the Institution of Civil Engineers – Structures and Buildings*, 176(2), 131–146.

Herath HMH, Jayaweerarathne DS, Wijesundara RSSA, Wijesundara KK (2023). Performance-based design method for bolted stiffened end-plate connection under monotonic loading. *Structures*, 53, 214–227.

Hu JW, Kim DK, Leon RT, Choi E (2011). Analytical studies of full-scale steel T-stub connections using delicate 3D finite element methods. *ISIJ International*, 51(4), 619–629.

Lee CH, Jung JH, Oh MH, Koo ES (2003). Cyclic seismic testing of steel moment connections reinforced with welded straight haunch. *Engineering Structures*, 25(14), 1743–1753.

Liu X, Sha X, Guo C, Wang Y, Zhang Z (2025). Simplified design methods of large-capacity moment end-plate connections. *Structures*, 78, 109095.

Liu Y, Zhang B, Liu X, Cheng T, Zhu H, Wang P, Liu F (2022). Seismic behavior investigation of TOB bolted endplate connection with novel internal strengthening structure. *Journal of Constructional Steel Research*, 190, 107141.

Morrison M, Suarez S (2022). Experiments and analysis of unstiffened eight-bolt end-plate moment connections for seismic applications. *Journal of Structural Engineering*, 148(4), 04022005.

Peng Z, Dai SB, Pi YL, Zhang YC, Huang J (2018). Seismic performance of end-plate connections between T-shaped CFST columns and RC beams. *Journal of Constructional Steel Research*, 145, 167–183.

Prinz GS, Nussbaumer A, Borges L, Khadka S (2014). Experimental testing and simulation of bolted beam-column connections having thick extended endplates and multiple bolts per row. *Engineering Structures*, 59, 434–447.

Saberi H, Saberi V, Kheyroddin A, Gerami M (2019). Seismic behavior of frames with bolted end plate connections rehabilitated by welded haunches under near- and far-fault earthquakes. *International Journal of Steel Structures*, 19(2), 672–691.

Taheripour M, Hatami F, Raoufi R (2022). Numerical study of two novel connections with short end I or H stub in steel structures. *Advanced Steel Construction*, 18(1), 495–505.

Troup S, Xiao RY, Moy SSJ (1998). Numerical modelling of bolted steel connections. *Journal of Constructional Steel Research*, 46(1–3), 269.

Xiao S, Bu X, Chen Y, Wang X (2024). Investigating the damage-based seismic performance of the blind bolt-connected steel framework. *Structures*, 69, 107388.

Yang JG, Lee GY (2007). Analytical models for the initial stiffness and ultimate moment of a double angle connection. *Engineering Structures*, 29(4), 542–551.

Yılmaz O, Bekiroğlu S (2016). The effect of reinforcing panel zone of bolted end plate column beam connections. *Journal of the Faculty of Engineering and Architecture of Gazi University*, 31(2), 241–253.

Yılmaz O, Bekiroğlu S (2022). Biaxial cyclic behavior of bolted end-plate connection to I-column reformed by box-plates. *Engineering Structures*, 255, 113955.

Zhang B, Yuan H, Xia C, Liu X, Liu M, Liu F, Wang P (2021). Seismic behavior of thread-fixed one-side bolted endplate connection of steel beam to hollow square column. *Journal of Building Engineering*, 43, 102557.

Zhang H, Zhou X, Ke K, Yam MCH, Shi Y, Zhang H (2023). Hybrid self-centering connection employing energy dissipation sequences: experimental study and a structural seismic demand perspective. *Journal of Structural Engineering*, 149(11), 04023157.

Zhang Y, Wang M, Shi G (2024). Mechanical behavior of the extended end-plate connections of a portal frame with various retrofitted constructions under loading. *Structures*, 63, 106477.

Zhang Y, Wang M, Shi G (2025a). A retrofit method for extended end-plate connections in portal frames using prefabricated cover plate components under loading. *Construction and Building Materials*, 475, 141205.

Zhang Y, Wang M, Shi G (2025b). Parametric analysis and design method of bolted extended end-plate beam-column connections in portal frames retrofitted with prefabricated cover plate components. *Journal of Building Engineering*, 111, 113399.

Zhao H, Shi G, Chen X, Xiao T (2021). Numerical simulation and mechanical model of steel beam-to-column joints retrofitted by haunches. *Journal of Constructional Steel Research*, 185, 106858.